




Bifurcations and Turing patterns in a diffusive Gierer–Meinhardt model

Yong Wang ¹, Mengping Guo¹ and Weihua Jiang²

¹Institute of Science and Technology, Tianjin University of Finance and Economics, Tianjin, China

²Department of Mathematics, Harbin Institute of Technology, Harbin, China

Received 30 August 2022, appeared 19 July 2023

Communicated by Roberto Livrea


Abstract. In this paper, the Hopf bifurcations and Turing bifurcations of the Gierer–Meinhardt activator-inhibitor model are studied. The very interesting and complex spatially periodic solutions and patterns induced by bifurcations are analyzed from both theoretical and numerical aspects respectively. Firstly, the conditions for the existence of Hopf bifurcation and Turing bifurcation are established in turn. Then, the Turing instability region caused by diffusion is obtained. In addition, to uncover the diffusion mechanics of Turing patterns, the dynamic behaviors are studied near the Turing bifurcation by using weakly nonlinear analysis techniques, and the type of spatial pattern was predicted by the amplitude equation. And our results show that the spatial patterns in the Turing instability region change from the spot, spot-stripe to stripe in order. Finally, the results of the analysis are verified by numerical simulations.

Keywords: Gierer–Meinhardt activator-inhibitor model, stability, Hopf bifurcation, Turing bifurcation, pattern.

2020 Mathematics Subject Classification: 34K18, 37G10, 35K57, 35B36.

1 Introduction

In general, reaction-diffusion systems [4, 14, 15] are used to describe models in which the concentration of one or more substances diffuses in space and is affected by the diffusion and inter-conversion of substances. In 1952, A. M. Turing [23] mathematically proposed the conclusion that the homogeneous steady state in a reaction-diffusion system becomes destabilized under certain conditions, that is, the initial steady-state solution of the reaction-diffusion system becomes unstable due to the introduction of a diffusion term. This instability caused by diffusion is often referred to as Turing instability. Thereafter, Turing instability has received a great amount of attention from a wide range of scholars and has become a typical problem in the formation of spatio-temporal patterns [1, 7, 9, 12, 16, 18, 21, 26]. The various results of pattern formation in the reaction-diffusion system are specified as follows. The Turing–Murray principle was proposed by James Murray [16], which investigated the reaction-diffusion systems

 Corresponding author. Email: ywang@tjufe.edu.cn

of animal bodies and tails and their Turing instability. Schepers and Markus [21] demonstrated that cellular automata can produce Turing patterns in the activator-inhibitor system that is qualitatively consistent with various experiments in chemistry. A diffusion model with a Degrn–Harrison reaction scheme is considered by Li et al. [12], and the local and global structure of the steady-state bifurcation is established by the technique of spatial decomposition and implicit function theorem. These works demonstrated that Turing patterns can emerge in a number of ecological and chemical systems.

To uncover the diffusion mechanism of Turing patterns and to examine the actual format of Turing patterns in the real world, we will select the activator-inhibitor model [6] proposed by Gierer and Meinhardt to study the typologies of Turing patterns. The activator-inhibitor model shows that two substances can resist each other's action, and can also be used to depict the formation of polar structures, animal structures, and periodic structures (dots on animals). In recent decades, a large literature has been devoted to the study of this system, as seen in [2, 11, 13, 20, 25] and the references therein, which can be written as

$$\begin{cases} \frac{\partial u}{\partial t} = \rho \frac{u^2}{v} - \mu_u u + D_u \frac{\partial^2 u}{\partial x^2} + \rho_u, \\ \frac{\partial v}{\partial t} = \rho u^2 - \mu_v v + D_v \frac{\partial^2 v}{\partial x^2} + \rho_v, \end{cases} \quad (1.1)$$

where

- (i) u and v represent the concentration of activator and inhibitor respectively, D_u and D_v are their corresponding diffusion constants, and $\frac{\partial u}{\partial t}$ means the change in the concentration of the activator per unit of time.
- (ii) $\rho_u > 0, \rho_v > 0$ represent the baseline yield of the activator and the inhibitor, separately, and μ_u, μ_v are the decay rate.

For the Gierer–Meinhardt system (1.1), Ruan [20] demonstrated that diffusion can cause homogeneous equilibrium solutions and homogeneous periodic solutions to become unstable. Liu et al. [13] investigated the multiple bifurcation analysis and spatiotemporal patterns in the one-dimensional Gierer–Meinhardt model. Wu et al. [25] performed a Hopf bifurcation analysis of this diffusion model and studied the direction and stability of Hopf bifurcation by standard central manifold theorem. Stability and Hopf bifurcation analysis on a simplified Gierer–Meinhardt model were studied by Asheghi [2], and the direction of the Hopf bifurcation was obtained by the normal form theory. The investigation conducted by Li et al. [11] pertained to the analysis of Turing patterns observed in a broad-spectrum Gierer–Meinhardt model of morphogenesis. In the particular case, when $\rho_u = \rho_v = 0$, a simple scale transformation model is as follows

$$\begin{cases} \frac{\partial u}{\partial t} = \sigma_1 \Delta u + \frac{u^2}{v} - \beta u & (x, y) \in \Omega, \quad t > 0, \\ \frac{\partial v}{\partial t} = \sigma_2 \Delta v + u^2 - v & (x, y) \in \Omega, \quad t > 0, \\ \partial_\nu u = \partial_\nu v = 0, & (x, y) \in \partial\Omega, \quad t > 0, \end{cases} \quad (1.2)$$

where

- (i) u and v stand for $u(x, y, t)$ and $v(x, y, t)$, $(x, y) \in \Omega \subset \mathbb{R}^2$, β denotes the decay rate of the activator.

- (ii) $\Delta = \frac{\partial^2}{\partial x^2} + \frac{\partial^2}{\partial y^2}$ is a common Laplace operator in two-dimensional space, and $\partial\Omega$ represents the homogeneous Neumann boundary condition.

None of the above-mentioned literature deals with the formation of Turing patterns on two-dimensional space in the Gierer–Meinhardt model. However, for chemical systems, patterns on a two-dimensional plane will be more realistic, more intuitive, and abundant than those on a one-dimensional plane [17,24]. For the one-dimensional space, only spot patterns and strip patterns exist. However, in two dimensions, not only spots and strips but also patterns such as spot-strip coexistence and maze shapes may appear. To more clearly understand the mechanisms of pattern formation in Gierer–Meinhardt model, we will study the spatio-temporal evolution pattern of the system (1.2) in two dimensions space.

In this paper, the dynamical behaviors of the system (1.2) are studied by using the decay rate of activator β as a bifurcation parameter. The existing conditions of the Hopf bifurcations and the Turing bifurcations are established in turn. The very interesting and complex patterns (spot patterns, spot-stripe coexistence patterns, and stripe patterns) induced by the Turing bifurcation are analyzed from both theoretical and numerical aspects by a multi-scale method [3,5,27]. And our results show that the decay rate of the activator β can affect the dynamical behavior of the system (1.2). The system will occur Turing instability when the decay rate β is within a certain region, the impact of diffusion on the system will be diminished as the decay rate β increases.

The layout of this paper is organized as follows. In Section 2, the conditions for the existence of Hopf bifurcation and the Turing instability with spatial inhomogeneity are discussed analytically. In Section 3, the amplitude equation near the instability threshold is derived using weakly nonlinear analysis, and different solutions to the amplitude equation and its stability are investigated. And the correctness of the theoretical part of the analysis is verified by numerical simulations in space. In Section 4, finally, some conclusions and discussions are given.

2 Turing instability and bifurcation analysis

In this section, the conditions for the existence of Hopf bifurcation and the Turing instability are discussed.

The local system corresponding to the diffusion system (1.2) is

$$\begin{cases} \frac{\partial u}{\partial t} = \frac{u^2}{v} - \beta u, \\ \frac{\partial v}{\partial t} = u^2 - v, \end{cases} \quad (2.1)$$

with a unique positive equilibrium

$$E_* = (U_*, V_*) = \left(\frac{1}{\beta}, \frac{1}{\beta^2} \right), \quad \beta > 0.$$

The Jacobian matrix computed. The Jacobi matrix taken at the positive equilibrium E_* is

$$A = \begin{pmatrix} \frac{\partial f}{\partial u} & \frac{\partial f}{\partial v} \\ \frac{\partial g}{\partial u} & \frac{\partial g}{\partial v} \end{pmatrix} = \begin{pmatrix} \beta & -\beta^2 \\ \frac{2}{\beta} & -1 \end{pmatrix} = \begin{pmatrix} a_{11} & a_{12} \\ a_{21} & a_{22} \end{pmatrix}, \quad (2.2)$$

and the characteristic equation is as follows

$$\lambda^2 - \text{tr}(A)\lambda + \text{Det}(A) = 0, \quad (2.3)$$

with

$$\begin{aligned} \operatorname{tr}(A) &= a_{11} + a_{22} = \beta - 1, \\ \operatorname{Det}(A) &= a_{11}a_{22} - a_{21}a_{12} = \beta. \end{aligned}$$

Theorem 2.1. *For the local system (2.1), when $0 < \beta < 1$, the positive equilibrium E_* is locally asymptotically stable, and the system (2.1) undergoes the Hopf bifurcation at $\beta = 1$.*

Proof. When $0 < \beta < 1$, obviously obtaining $\operatorname{tr}(A) < 0$ and $\operatorname{Det}(A) > 0$, hence, the positive equilibrium E_* is locally asymptotically stable. When $\beta = 1$, then $\operatorname{tr}(A) = 0$ and $\operatorname{Det}(A) > 0$, the system (2.1) undergoes Hopf bifurcation. Next, we verify the transversality condition for the Hopf bifurcation at $\beta = 1$

$$\left. \frac{d\operatorname{Re}\lambda_0(\beta)}{d\beta} \right|_{\beta=1} = \frac{1}{2} > 0.$$

According to the Poincaré–Andronov–Hopf bifurcation theorem [19], the system (2.1) undergoes a Hopf bifurcation when $\beta = 1$. \square

Next, we study the diffusion-driven Turing instability of the diffusion system (1.2) under the basic assumption that the constant equilibrium $E_*(u_*, v_*)$ of the system (1.2) is asymptotically stable ($0 < \beta < 1$).

In order to study the linear stability of the constant equilibrium $E_*(u_*, v_*)$ of (1.2), we need to study the distribution of the roots of the characteristic equation of (1.2). The linearization of Equation (1.2) at the constant equilibrium point $E_*(u_*, v_*)$ is

$$\begin{pmatrix} \frac{\partial u}{\partial t} \\ \frac{\partial v}{\partial t} \\ \frac{\partial \theta}{\partial t} \end{pmatrix} = \begin{pmatrix} \sigma_1 \Delta & 0 \\ 0 & \sigma_2 \Delta \end{pmatrix} \begin{pmatrix} u \\ v \end{pmatrix} + A \begin{pmatrix} u \\ v \end{pmatrix}. \quad (2.4)$$

Assume the solution of (2.4) is that

$$\begin{pmatrix} u \\ v \end{pmatrix} = \begin{pmatrix} u^* \\ v^* \end{pmatrix} + \begin{pmatrix} u_k \\ v_k \end{pmatrix} \exp(\lambda t + i(\mathbf{k} \cdot \mathbf{r})), \quad (2.5)$$

where \mathbf{k} denotes the wave number with the expression $\mathbf{k} = (k_x, k_y)$, and satisfies $k = |\mathbf{k}|$. \mathbf{r} is the spatial vector in two dimensions whose expression is $\mathbf{r} = (x, y)$. We can get the corresponding characteristic matrix is

$$A_k = \begin{pmatrix} a_{11} - \sigma_1 k^2 & a_{12} \\ a_{21} & a_{22} - \sigma_2 k^2 \end{pmatrix}.$$

The characteristic equation is

$$F_k(\lambda) = \lambda^2 - T_k \lambda + D_k = 0, \quad (2.6)$$

where

$$\begin{aligned} T_k &= \beta - 1 - k^2(\sigma_1 + \sigma_2), \\ D_k &= \sigma_1 \sigma_2 k^4 - (-\sigma_1 + \sigma_2 \beta) k^2 + \beta. \end{aligned} \quad (2.7)$$

Under Theorem 2.1, we have $0 < \beta < 1$, thus for any positive natural number k , there always exist $T_k < 0$. Then the instability condition of the positive equilibrium point $E_*(u_*, v_*)$ of the system (1.2) should be that: existing a $k > 0$ make $D_k < 0$. In other words, when $D_k < 0$

($k > 0$) is satisfied, there exists a diffusion-driven Turing instability. Since $\beta > 0$, the sufficient condition for $D_k < 0$ is that the following two conditions H_1 and H_2 hold

$$H_1 : -\sigma_1 + \sigma_2\beta > 0,$$

and

$$H_2 : (\sigma_1 - \sigma_2\beta)^2 - 4\beta\sigma_1\sigma_2 > 0.$$

Consider D_k as a quadratic function of k^2 , the function D_k can obtain the minimum value at k_T , where $k_T^2 = \sqrt{\frac{\beta}{\sigma_1\sigma_2}}$. If H_1 and H_2 hold, then $\min D_{k_T} < 0$, which indicates the occurrence of Turing instability.

In the following, we choose β as the parameter to study the conditions that make H_1 and H_2 hold. Regarding the Turing instability of the system (1.2), we obtain the following results.

Theorem 2.2. *Assume that the positive equilibrium point E_* of the corresponding local system (2.1) is stable, which is given by Theorem 2.1. For the reaction-diffusion system (1.2)*

(I) *if $\sigma_1 \geq \sigma_2$, there is no Turing instability;*

(II) *if $\sigma_1 < \sigma_2$, the following results are achieved*

(i) *when $\beta_T^{(2)} > 1$, there is no Turing instability;*

(ii) *when $\beta_T^{(2)} < 1$, Turing instability occurs at $\beta \in (\beta_T^{(2)}, 1)$ and Turing bifurcation occurs at $\beta = \beta_T^{(2)}$,*

where

$$\beta_T^{(2)} = \frac{(3 + 2\sqrt{2})\sigma_1}{\sigma_2}.$$

Proof. (I) From Theorem 2.1, we know that the positive equilibrium point E_* is stable for $0 < \beta < 1$. Therefore, when $\sigma_1 \geq \sigma_2$, we have $\frac{\sigma_1}{\sigma_2} \geq 1 > \beta$, hence H_1 is not satisfied. The conclusion (I) is proved.

(II) Under the conditions of Theorem 2.1, it is easy to get H_1 equivalent to $\beta_* < \beta < 1$, where

$$\beta_* = \frac{\sigma_1}{\sigma_2}, \quad (2.8)$$

and H_2 is equivalent to the following condition

$$h(\beta) = \sigma_2^2\beta^2 - 6\sigma_1\sigma_2\beta + \sigma_1^2 > 0. \quad (2.9)$$

Let

$$Q_1 = (-6\sigma_1\sigma_2)^2 - 4\sigma_2^2\sigma_1^2 = 32\sigma_1^2\sigma_2^2, \quad (2.10)$$

obviously, $Q_1 > 0$. This means that $h(\beta) = 0$ has two positive roots, which are denoted as $\beta_T^{(1)}$ and $\beta_T^{(2)}$

$$0 < \beta_T^{(1)} = \frac{(3 - 2\sqrt{2})\sigma_1}{\sigma_2} < \beta_T^{(2)} = \frac{(3 + 2\sqrt{2})\sigma_1}{\sigma_2}, \quad (2.11)$$

and $h(\beta) > 0$ if only and if $0 < \beta < \beta_T^{(1)}$ and $\beta > \beta_T^{(2)}$. In addition, we can get

$$h(\beta_*) = \sigma_2^2 \frac{\sigma_1^2}{\sigma_2^2} - 6\sigma_1\sigma_2 \frac{\sigma_1}{\sigma_2} + \sigma_1^2 = -4\sigma_1^2 < 0,$$

hence, we have the following inequality,

$$0 < \beta_T^{(1)} < \beta_* < \beta_T^{(2)}. \quad (2.12)$$

Therefore, H_1, H_2 are both satisfied for $\beta_T^{(2)} < \beta < 1$, not satisfied for $0 < \beta < \beta_T^{(1)}$, H_1, H_2 . Then we can conclude that Turing instability occurs only in the region $\beta_T^{(2)} < \beta < 1$, which completes the proof of (ii) in Conclusion (II).

Furthermore, if $\beta_T^{(2)} > 1$, the positive equilibrium point E_* is unstable, hence, there is no Turing instability. The conclusion (i) in (II) is proved. \square

To support the previous theoretical analysis, taking $\sigma_1 = 0.3, \sigma_2 = 5$, we can obtain $\beta_T^{(2)} = 0.3497$. According to [Theorem 2.2](#), we know that Turing instability occurs for $\beta \in (\beta_T^{(2)}, 1)$. Therefore, to investigate the Turing pattern formation of system (1.2), we need to ensure that the control parameter $\beta \in (0.3497, 1)$. By increasing the value of parameter β in $(0.3497, 1)$, we can obtain the relationship between $Re(\lambda)$ and k^2 (see [Figure 2.1\(a\)](#)) and the relationship between D_k and k^2 (see [Figure 2.1\(b\)](#)), where $Re(\lambda)$ is the real part of λ . From [Figure 2.1\(a\)](#) and [Figure 2.1\(b\)](#), it is easy to see that $Re(\lambda) < 0$ and $D_k > 0$ always hold for $\beta < \beta_T^{(2)}$, which implies that there is no Turing instability. Therefore, $\beta > \beta_T^{(2)}$ is the necessary condition for Turing instability to occur.

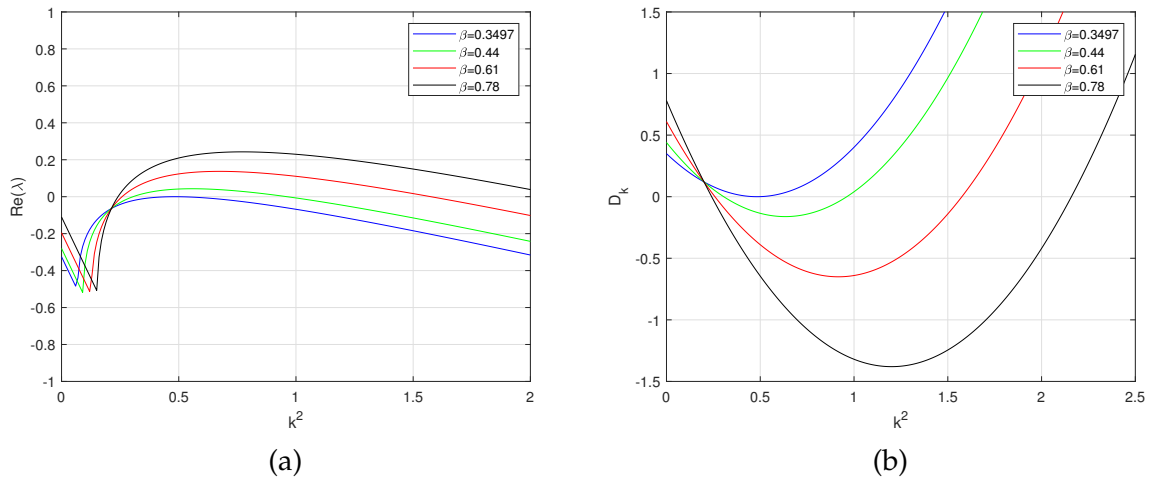


Figure 2.1: (a): the graph of the dispersion relation with respect to k^2 for different β ; (b): the graph of $D_k(\beta)$ with respect to k^2 for different β .

In the following, we consider the Hopf bifurcation of the system (1.2) around $E(u_*, v_*)$. By [Theorem 2.1](#), when $0 < \beta < 1$, then $T_0 = \beta - 1 < 0$ and $T_k = T_0 - k^2(\sigma_1 + \sigma_2) < 0$ for any $k \geq 0$. Let $k = \frac{n}{l}$, $n \in \mathbb{N}_0, l \in \mathbb{R}^+$. According to [8], n -mode Hopf bifurcation means that the characteristic equation (2.6) has a pair of purely imaginary roots, while the other roots have non-zero real parts and satisfy the corresponding transversal conditions.

Theorem 2.3. *Suppose one of the following conditions holds:*

- (I) $0 < \beta \leq \beta_*$;
- (II) $\beta > \beta_T^{(2)}$.

The system (1.2) occurs 0-mode Hopf bifurcation at $\beta = \beta_0^H = 1$, where the characteristic $F_0(\lambda) = 0$ have a pair of purely imaginary roots and other roots of the characteristic $F_k(\lambda) = 0$ ($k > 0$) have negative real parts. Where β_* and $\beta_T^{(2)}$ are defined in (2.8) and (2.11).

Proof. Since $\frac{dT_0}{d\beta} = \frac{1}{2}$, then $T_0 = 0$ has a unique root $\beta = \beta_0^H = 1$, and obviously the transversal conditions satisfied. Moreover, $T_k < 0$ ($k \geq 1$) and $D_0 = \beta > 0$. Since $-\sigma_1 + \sigma_2\beta \leq 0$, then $0 < \beta \leq \beta_*$. It is easy to obtain that $D_k > 0$ always holds for $0 < \beta \leq \beta_*$. When $-\sigma_1 + \sigma_2\beta > 0$, according (2.10) we know that $D_k > 0$ is equivalent to conditions $0 < \beta < \beta_T^{(1)}$ or $\beta > \beta_T^{(2)}$ holding. Combining (2.12), it is find that $\beta > \beta_T^{(2)}$ usable $D_k > 0$ always satisfied. Thus the system (1.2) occurs 0-mode Hopf bifurcation. \square

In the next, we find the spatially inhomogeneous Hopf bifurcation for $n \in \mathbb{N}$. Define

$$\beta_n^H = 1 + \left(\frac{n}{l}\right)^2 (\sigma_1 + \sigma_2), \quad (2.13)$$

which is the root of $T_{\frac{n}{l}} = \beta - 1 - \left(\frac{n}{l}\right)^2(\sigma_1 + \sigma_2) = 0$. There are the following conclusions.

Theorem 2.4. *Suppose one of the following conditions holds:*

- (I) $0 < \beta \leq \beta_*$;
- (II) $\beta > \beta_T^{(2)}$.

The system (1.2) undergoes a n -mode Hopf bifurcation around $E_*(u_*, v_*)$ at β_n^H for $n \in \mathbb{N}$, where the characteristic equation (2.6) has a pair of purely imaginary roots, while all the other roots of $F_j(\lambda) = 0$ ($j \neq \frac{n}{l}$) have non-zero real parts. Where β_* and $\beta_T^{(2)}$ are defined in (2.8) and (2.11).

Proof. To find the spatially inhomogeneous Hopf bifurcation points for $n \in \mathbb{N}$, we have to seek the roots of $\left(\frac{n}{l}\right)^2(\sigma_1 + \sigma_2) + 1 = \beta$. Since $\frac{dT_{\frac{n}{l}}}{d\beta} = \frac{1}{2}$, then $T_{\frac{n}{l}} = 0$ has a unique root $\beta = \beta_n^H$ for $n \in \mathbb{N}$, and obviously the corresponding transversal conditions satisfied. Moreover, it is easy to get that $T_{\frac{n}{l}}$ is monotonically decreasing with respect to n , therefore $T_{\frac{j}{l}}(\beta_n^H) > 0$ for $j < n$ and $T_{\frac{j}{l}}(\beta_n^H) < 0$ for $j > n$. By the proof of Theorem 2.3, we know that $D_k > 0$ for one of the conditions in (I) or (II) holds. Thus the system undergoes n -mode Hopf bifurcation at β_n^H . \square

In addition, to more intuitively understand Theorem Theorem 2.2–Theorem 2.4, taking $\sigma_1 = 0.4$, we plot the stability regions and the existing region of Turing instability in $\sigma_2 - \beta$ plane, as shown in Figure 2.2. According to Theorem 2.1–Theorem 2.4, in D_1 , the positive equilibrium E_* is unstable and occurs Turing instability, and $\beta = \beta_T^{(2)}$ represents Turing bifurcation curve. In D_2 , the positive equilibrium E_* is unstable but not occurs Turing instability. In D_3 and D_4 the positive equilibrium E_* is asymptotically stable. Moreover, we set $\sigma_1 = 0.4$, $\sigma_2 = 0.2$, then the 0-mode Hopf bifurcation will occurs at $\beta = \beta_0^H = 1$. Taking $\beta = 0.99 < \beta_0^H$, the system (1.2) can occur the spatially homogeneous periodic solutions (as shown in Figure 2.3). We set $\sigma_1 = 0.4$, $\sigma_2 = 3$, $n = 1$, $l = 8$, thus $\beta_1^H = 1.0531$. And the 1-mode Hopf bifurcation will occurs at $\beta = \beta_1^H$. Taking $\beta = 1.01 < \beta_1^H$, the system (1.2) can appear the spatially inhomogeneous periodic solution (as shown in Figure 2.4).

Remark 2.5. When $\beta \in (\beta_*, \beta_T^{(2)})$, at least one eigenvalue of D_k has positive real part, then the Hopf bifurcating periodic solutions are always unstable. Particularly, for 0-mode Hopf bifurcation, bifurcating periodic solutions are unstable in the interval AB in Figure 2.2.

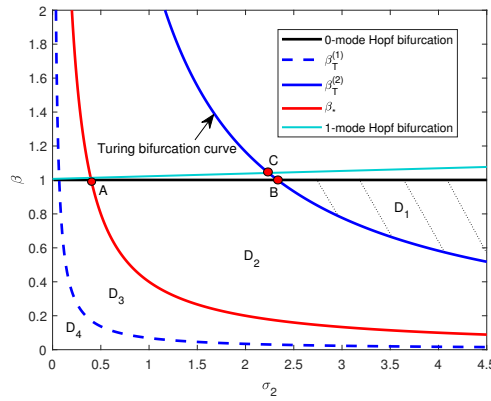


Figure 2.2: When $\sigma_1 = 0.4$, the Turing bifurcation curve and Hopf bifurcation curve in $\sigma_2 - \beta$ plane. D_1 is the Turing instability region, D_2 denotes unstable regions in which do not occurs Turing unstable, D_3 and D_4 are both stable regions. And B represents $(k_T, 0)$ -mode Turing–Hopf bifurcation point, C stands for $(k_T, 1)$ -mode Turing–Hopf bifurcation point.

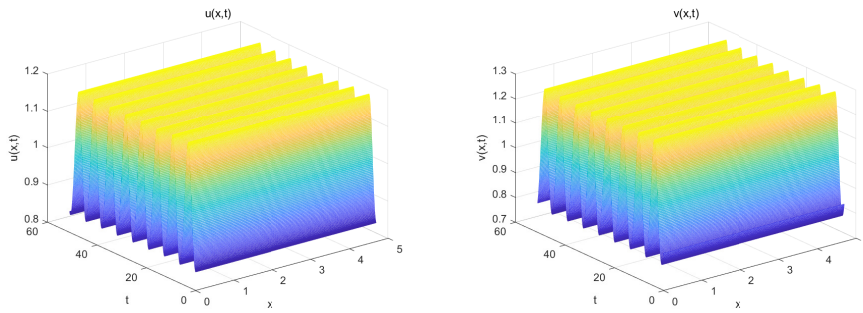


Figure 2.3: The spatially homogeneous periodic solution with $\sigma_1 = 0.4$, $\sigma_2 = 0.2$, $\beta = 0.99$. The initial values is $(u_0, v_0) = (0.85, 0.85)$, and $0 \leq x \leq 5$, $0 \leq t \leq 60$.

Remark 2.6. In Figure 2.2, B and C denote the Turing–Hopf bifurcation points corresponding to the $(k_T, 0)$ -mode and $(k_T, 1)$ -mode, respectively. Point B is located at the coordinates $(2.33, 1)$, while point C is located at $(2.24, 1.041)$. To investigate the dynamical behaviors that may occur near these points, we performed numerical simulations. Notably, in the vicinity of point B and C , we observe spatially homogeneous periodic solutions, non-constant steady-state solutions and spatially homogeneous quasi-periodic solutions. These observations are visually depicted in Figure 2.5. These results provide valuable insights into the behavior of the system near the Turing–Hopf bifurcation point.

This section focuses on the stability, Hopf bifurcation, and Turing instability regions of the diffusive Gierer–Meinhardt activator-inhibitor system (1.2) and obtains the conditions for the occurrence of Turing bifurcation, 0-mode Hopf bifurcation, k -mode Hopf bifurcation. As it is known, pattern formation can be induced by Turing instability. To uncover the diffusion mechanics of Turing patterns, this paper requires us to investigate and analyze the dynamic behavior of the Turing bifurcation. To solve this problem, we will employ the amplitude equation as an effective tool. In the next section, we will consider the amplitude equation of the system (1.2).

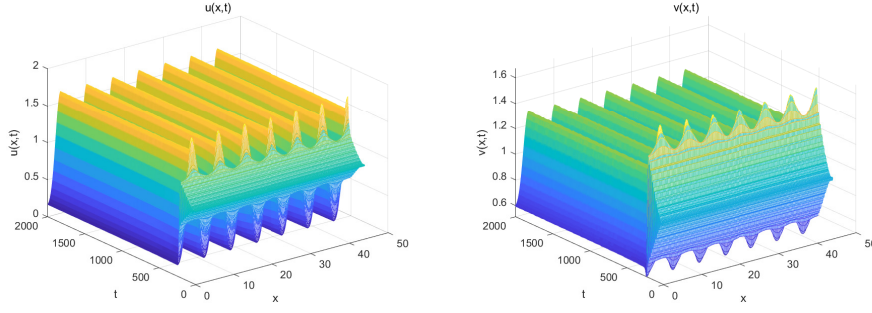


Figure 2.4: The spatially inhomogeneous periodic solution with $\sigma_1 = 0.4$, $\sigma_2 = 3$, $\beta = 1.01$. The initial values is $(u_0, v_0) = (0.99, 0.99)$, and $0 \leq x \leq 50$, $0 \leq t \leq 2000$.

3 The amplitude equation and pattern formation

3.1 The amplitude equation of Turing bifurcation

In this subsection, in order to reveal the effect of diffusion on Turing patterns, the amplitude equation of the system (1.2) near the Turing bifurcation $\beta = \beta_T^{(2)}$ will be deduced by weakly nonlinear analysis [3, 5, 27]. To begin with, we consider the third order polynomial system of the system (1.2), which can be expressed as

$$\frac{\partial U}{\partial t} = IU + S(U, U), \quad (3.1)$$

where

$$U = \begin{pmatrix} u \\ v \end{pmatrix}, \quad I = \begin{pmatrix} a_{11} + \sigma_1 \Delta & a_{12} \\ a_{21} & a_{22} + \sigma_2 \Delta \end{pmatrix},$$

and

$$S = \begin{pmatrix} f_{uu}u^2 + f_{uv}uv + f_{vv}v^2 \\ g_{uv}u^2 + g_{uv}uv + g_{uv}v^2 \end{pmatrix} + \begin{pmatrix} f_{uuu}u^3 + f_{uuv}u^2v + f_{uvv}uv^2 + f_{vvv}v^3 \\ g_{uuu}u^3 + g_{uuv}u^2v + g_{uvv}uv^2 + g_{vvv}v^3 \end{pmatrix} + o(4).$$

Applying perturbation techniques to the system (3.1), a small parameter ε is introduced near the critical value $\beta_T^{(2)}$ of the Turing bifurcation and satisfies the following form

$$\beta - \beta_T^{(2)} = \varepsilon\beta_1 + \varepsilon^2\beta_2 + \varepsilon^3\beta_3 + o(\varepsilon^3).$$

Meanwhile, the linear operator I can be decomposed into

$$I_\varepsilon = I_T + (\varepsilon\beta_1 + \varepsilon^2\beta_2 + \dots) C, \quad (3.2)$$

where

$$I_T = \begin{pmatrix} a_{11}^T & a_{12}^T \\ a_{21}^T & a_{22}^T \end{pmatrix}, \quad (3.3)$$

$$C = \begin{pmatrix} c_{11} & c_{12} \\ c_{21} & c_{22} \end{pmatrix} = \begin{pmatrix} 1 & -2\beta_T^{(2)} \\ -\frac{2}{(\beta_T^{(2)})^2} & 0 \end{pmatrix},$$

with

$$a_{ij}^T = a_{ij}|_{\beta=\beta_T^{(2)}}, \quad c_{ij} = \frac{a_{ij}}{d\beta}.$$

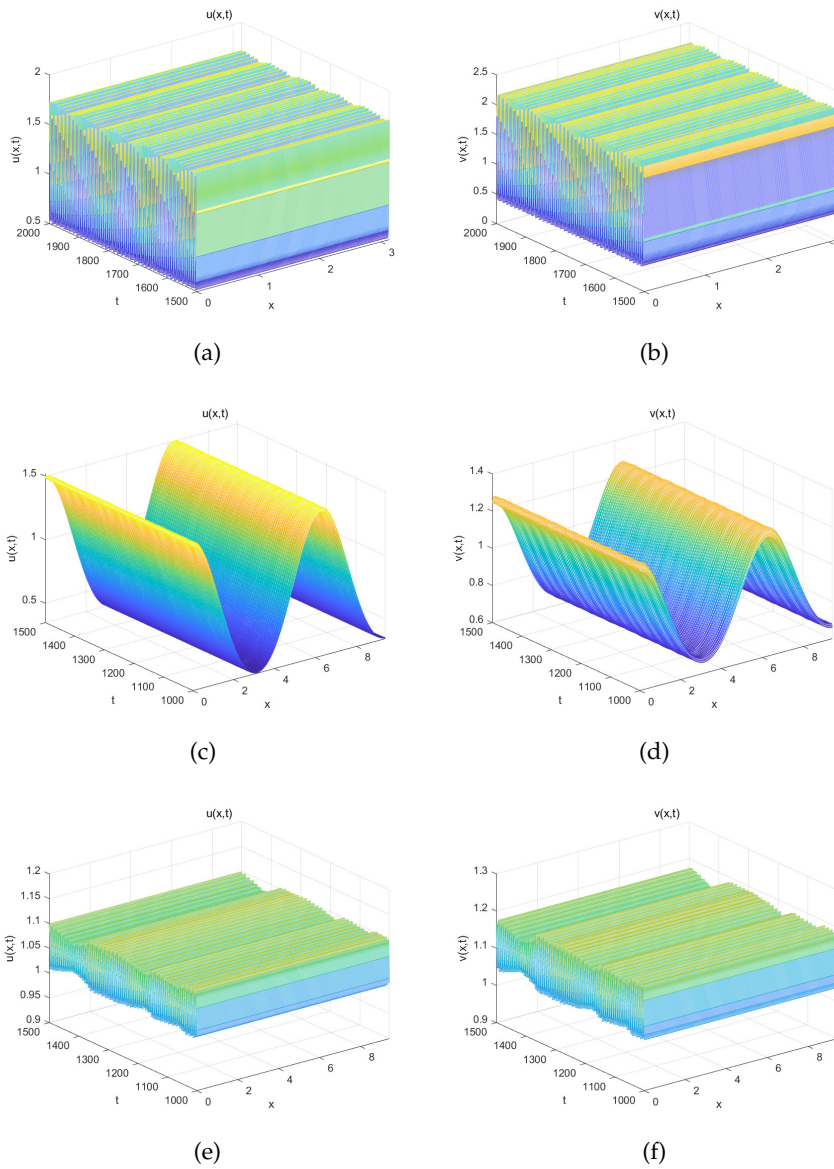


Figure 2.5: (a) and (b) are spatially homogeneous periodic solutions with $\sigma_1 = 0.4$, $\sigma_2 = 2.5$, $\beta = 1.002$, and $0 \leq x \leq 3$, $1500 \leq t \leq 2000$; (c) and (d) represent non-constant steady-state solutions with $\sigma_1 = 0.4$, $\sigma_2 = 2.43$, $\beta = 0.99$, and $0 \leq x \leq 8$, $1000 \leq t \leq 1500$; (e) and (f) correspond to spatially homogeneous quasi-periodic solutions with $\sigma_1 = 0.4$, $\sigma_2 = 2.25$, $\beta = 0.95$, and $0 \leq x \leq 8$, $1000 \leq t \leq 1500$. In all cases, the initial values for u and v are given by $(u_0, v_0) = (0.9 + 0.01 \cos(2x), 0.9 + 0.01 \cos(2x))$.

In addition, relating the variable U to the parameter ε can be written as

$$\mathbf{U} = \begin{pmatrix} u \\ v \end{pmatrix} = \varepsilon \begin{pmatrix} u_1 \\ v_1 \end{pmatrix} + \varepsilon^2 \begin{pmatrix} u_2 \\ v_2 \end{pmatrix} + \varepsilon^3 \begin{pmatrix} u_3 \\ v_3 \end{pmatrix} + o(\varepsilon^3). \quad (3.4)$$

Substituting (3.2) and (3.4) into system (3.1), we obtain the following equation

$$\frac{\partial \mathbf{U}}{\partial t} = \mathcal{I}_\varepsilon \mathbf{U} + \mathcal{S}(\mathbf{U}, \varepsilon), \quad (3.5)$$

where

$$\mathcal{I}_\varepsilon = \begin{pmatrix} \sigma_1 \Delta & 0 \\ 0 & \sigma_2 \Delta \end{pmatrix} + I_\varepsilon, \quad S(U, \varepsilon) = \varepsilon^2 S_2 + \varepsilon^3 S_3 + o(\varepsilon^3), \quad (3.6)$$

particularly,

$$\mathcal{I}_0 = I_T + \begin{pmatrix} \sigma_1 \Delta & 0 \\ 0 & \sigma_2 \Delta \end{pmatrix}.$$

Accordingly, multiple time scales are introduced and the derivatives with respect to t are converted to

$$\frac{\partial}{\partial t} = \varepsilon \frac{\partial}{\partial T_1} + \varepsilon^2 \frac{\partial}{\partial T_2} + \varepsilon^3 \frac{\partial}{\partial T_3} + o(\varepsilon^3). \quad (3.7)$$

Substitute (3.1)-(3.7) into (3.5), then deriving the coefficients of ε^j ($j = 1, 2, 3$) satisfies the following equation

$O(\varepsilon)$:

$$\mathcal{I}_0 \begin{pmatrix} u_1 \\ v_1 \end{pmatrix} = 0, \quad (3.8)$$

$O(\varepsilon^2)$:

$$\mathcal{I}_0 \begin{pmatrix} u_2 \\ v_2 \end{pmatrix} = \frac{\partial}{\partial T_1} \begin{pmatrix} u_1 \\ v_1 \end{pmatrix} - \beta_1 C \begin{pmatrix} u_1 \\ v_1 \end{pmatrix} - S_2, \quad (3.9)$$

$O(\varepsilon^3)$:

$$\mathcal{I}_0 \begin{pmatrix} u_3 \\ v_3 \end{pmatrix} = \frac{\partial}{\partial T_1} \begin{pmatrix} u_2 \\ v_2 \end{pmatrix} + \frac{\partial}{\partial T_2} \begin{pmatrix} u_1 \\ v_1 \end{pmatrix} - \beta_1 C \begin{pmatrix} u_2 \\ v_2 \end{pmatrix} - \beta_2 C \begin{pmatrix} u_1 \\ v_1 \end{pmatrix} - S_3, \quad (3.10)$$

where

$$S_2 = \begin{pmatrix} s_{21} \\ s_{22} \end{pmatrix}, \quad S_3 = \begin{pmatrix} s_{31} \\ s_{32} \end{pmatrix},$$

with

$$\begin{aligned} s_{21} &= \frac{1}{2} f_{uu} u_1^2 + \frac{1}{2} (f_{uv} + f_{vu}) u_1 v_1 + \frac{1}{2} f_{vv} v_1^2, \\ s_{31} &= \frac{1}{6} f_{uuu} u_1^3 + \frac{1}{6} f_{vvv} v_1^3 + \frac{1}{6} (f_{uuv} + f_{vuu} + f_{vu}) u_1^2 v_1 + f_{uu} u_2 u_1 + f_{vv} v_2 v_1 \\ &\quad + \frac{1}{6} (f_{uvv} + f_{vuv} + f_{vvu}) u_1 v_1^2 + \frac{1}{2} (f_{uv} + f_{vu}) (u_2 v_1 + u_1 v_2), \end{aligned}$$

s_{22} and s_{32} can be obtained by replacing f by g in s_{21} and s_{31} , and

$$\begin{aligned} f_{uu} &= \frac{2}{v}, & f_{uv} &= -\frac{2u}{v^2}, & f_{uuv} &= -\frac{2}{v^2}, & f_{uvv} &= \frac{4u}{v^3}, \\ f_{vu} &= -\frac{2u}{v^2}, & f_{vv} &= \frac{2u^2}{v^3}, & f_{vvv} &= -\frac{6u^2}{v^4}, & g_{uu} &= 2, \\ f_{vuu} &= -\frac{2}{v^2}, & f_{vuv} &= \frac{4u}{v^3}, & f_{vvu} &= \frac{4u}{v^3}, & f_{vuu} &= -\frac{2}{v^2}. \end{aligned}$$

Firstly, we discuss the first order of ε , while $(u_1, v_1)^T$ is the linear combinations that belong to the eigenvectors corresponding to zero eigenvalues. The general solution of equation (3.9) can be composed in the following form

$$\begin{pmatrix} u_1 \\ v_1 \end{pmatrix} = \begin{pmatrix} \phi \\ 1 \end{pmatrix} \left(\sum_{j=1}^3 M_j \exp(i\mathbf{k}_j \mathbf{r}) + \sum_{j=1}^3 \bar{M}_j \cdot \exp(-i\mathbf{k}_j \mathbf{r}) \right), \quad (3.11)$$

where the wave numbers satisfy $\mathbf{k}_1 + \mathbf{k}_2 + \mathbf{k}_3 = 0$, and $|\mathbf{k}| = k_T$. By substituting (3.11) into (3.8), we can get

$$\mathcal{I}_0 \begin{pmatrix} \phi \\ 1 \end{pmatrix} \exp(i\mathbf{k}_j \mathbf{r}) = \begin{pmatrix} a_{11} - \sigma_1 k_T^2 & a_{12} \\ a_{21} & a_{22} - \sigma_2 k_T^2 \end{pmatrix} \begin{pmatrix} \phi \\ 1 \end{pmatrix} = 0 \quad (3.12)$$

For convenience, we define

$$\mathcal{C}_k = \begin{pmatrix} a_{11} - \sigma_1 k_T^2 & a_{12} \\ a_{21} & a_{22} - \sigma_2 k_T^2 \end{pmatrix}.$$

It is clear that $(\phi, 1)^T$ is a zero eigenvector of \mathcal{C}_k , and by simple calculation, we can obtain $\phi = \frac{\sigma_2 k_T^2 - a_{22}}{a_{21}}$.

Using the Fredholm solvability condition for (3.10), the zero eigenvectors of the adjoint operator I_T^* of I_T is orthogonal to (3.10) right-hand side, and the eigenvector corresponding to the zero eigenvalues of I_T^* is

$$\begin{pmatrix} 1 \\ \varphi \end{pmatrix} \cdot \exp(-i\mathbf{k}_j \mathbf{r}) + c.c., \quad (3.13)$$

which follows

$$(1, \varphi) \cdot \mathcal{C}_k^T = 0, \quad (3.14)$$

with $\varphi = \frac{\sigma_1 k_T^2 - a_{11}}{a_{12}}$.

Using the Fredholm solvability condition to (3.10)

$$(1, \varphi) \cdot \left[\frac{\partial}{\partial T_1} \begin{pmatrix} u_1 \\ v_1 \end{pmatrix} - \beta_1 \mathcal{C} \begin{pmatrix} u_1 \\ v_1 \end{pmatrix} - S_2 \right] = 0. \quad (3.15)$$

By moving the term, we get the following formula

$$(1, \varphi) \cdot \frac{\partial}{\partial T_1} \begin{pmatrix} u_1 \\ v_1 \end{pmatrix} = (1, \varphi) \cdot \left[\beta_1 \mathcal{C} \begin{pmatrix} u_1 \\ v_1 \end{pmatrix} + S_2 \right].$$

Using the orthogonality condition for (3.10), we can obtain the following equations

$$\begin{cases} (\phi + \varphi) \frac{\partial M_1}{\partial T_1} = \left(\phi - 2\beta^T - \frac{2\phi\varphi}{(\beta^T)^2} \right) \beta_1 M_1 + 2(1, \varphi) \begin{pmatrix} s_1 \\ s_2 \end{pmatrix} \cdot \bar{M}_2 \cdot \bar{M}_3, \\ (\phi + \varphi) \frac{\partial M_2}{\partial T_1} = \left(\phi - 2\beta^T - \frac{2\phi\varphi}{(\beta^T)^2} \right) \beta_1 M_2 + 2(1, \varphi) \begin{pmatrix} s_1 \\ s_2 \end{pmatrix} \cdot \bar{M}_1 \cdot \bar{M}_3, \\ (\phi + \varphi) \frac{\partial M_3}{\partial T_1} = \left(\phi - 2\beta^T - \frac{2\phi\varphi}{(\beta^T)^2} \right) \beta_1 M_3 + 2(1, \varphi) \begin{pmatrix} s_1 \\ s_2 \end{pmatrix} \cdot \bar{M}_1 \cdot \bar{M}_2, \end{cases} \quad (3.16)$$

where

$$s_1 = \frac{f_{uu}}{2} \phi^2 + \frac{(f_{uv} + f_{vu})}{2} \phi + \frac{f_{vv}}{2}, \quad s_2 = \frac{g_{uu}}{2} \phi^2 + \frac{(g_{uv} + g_{vu})}{2} \phi + \frac{g_{vv}}{2}.$$

Suppose that the solution of (3.10) has the following form

$$\begin{pmatrix} u_2 \\ v_2 \end{pmatrix} = \begin{pmatrix} U_0 \\ V_0 \end{pmatrix} + \sum_{j=1}^3 \begin{pmatrix} U_j \\ V_j \end{pmatrix} e^{i\mathbf{k}_j \mathbf{r}} + \sum_{j=1}^3 \begin{pmatrix} U_{jj} \\ V_{jj} \end{pmatrix} e^{i2\mathbf{k}_j \mathbf{r}} + \begin{pmatrix} U_{12} \\ V_{12} \end{pmatrix} e^{i(\mathbf{k}_1 - \mathbf{k}_2) \mathbf{r}} \\ + \begin{pmatrix} U_{23} \\ V_{23} \end{pmatrix} e^{i(\mathbf{k}_2 - \mathbf{k}_3) \mathbf{r}} + \begin{pmatrix} U_{31} \\ V_{31} \end{pmatrix} e^{i(\mathbf{k}_3 - \mathbf{k}_1) \mathbf{r}} + c.c. \quad (3.17)$$

where $c.c$ represents the complex conjugate of all the preceding terms. Substituting (3.17) into (3.10), we can derive that

$$\begin{aligned} \begin{pmatrix} U_0 \\ V_0 \end{pmatrix} &= \begin{pmatrix} u_0 \\ v_0 \end{pmatrix} (|M_1|^2 + |M_2|^2 + |M_3|^2), \quad U_j = \phi V_j, \\ \begin{pmatrix} U_{jj} \\ V_{jj} \end{pmatrix} &= \begin{pmatrix} u_{11} \\ v_{11} \end{pmatrix} M_j^2, \quad \begin{pmatrix} U_{mn} \\ V_{mn} \end{pmatrix} = \begin{pmatrix} u_{mn} \\ v_{mn} \end{pmatrix} M_m \bar{M}_n, \end{aligned}$$

where

$$\begin{aligned} \begin{pmatrix} u_0 \\ v_0 \end{pmatrix} &= \frac{1}{a_{11}a_{22} - a_{12}a_{21}} \begin{pmatrix} -a_{22}s_1 + a_{12}s_2 \\ -a_{11}s_2 + a_{21}s_1 \end{pmatrix}, \\ \begin{pmatrix} u_{11} \\ v_{11} \end{pmatrix} &= \frac{1}{2} \frac{1}{(a_{11} - 4k_T^2\sigma_1)(a_{22} - 4k_T^2\sigma_2) - a_{12}a_{21}} \begin{pmatrix} -(a_{22} - 4k_T^2\sigma_2)s_1 + a_{12}s_2 \\ -(a_{11} - 4k_T^2\sigma_1)s_2 + a_{21}s_1 \end{pmatrix}, \\ \begin{pmatrix} u_{mn} \\ v_{mn} \end{pmatrix} &= \frac{1}{(a_{11} - 3k_T^2\sigma_1)(a_{22} - 3k_T^2\sigma_2) - a_{12}a_{21}} \begin{pmatrix} -(a_{22} - 3k_T^2\sigma_2)s_1 + a_{12}s_2 \\ -(a_{11} - 3k_T^2\sigma_1)s_2 + a_{21}s_1 \end{pmatrix}. \end{aligned}$$

Using the Fredholm solvability condition to (3.10),

$$(1, \varphi) \cdot \left[\frac{\partial}{\partial T_1} \begin{pmatrix} u_2 \\ v_2 \end{pmatrix} + \frac{\partial}{\partial T_2} \begin{pmatrix} u_1 \\ v_1 \end{pmatrix} - \beta_1 C \begin{pmatrix} u_2 \\ v_2 \end{pmatrix} - \beta_2 C \begin{pmatrix} u_1 \\ v_1 \end{pmatrix} - S_3 \right] = 0. \quad (3.18)$$

After simplification, we can obtain the following equations

$$\begin{cases} (\phi + \varphi) \left(\frac{\partial V_1}{\partial T_1} + \frac{\partial M_1}{\partial T_2} \right) = s_3 (\beta_1 V_1 + \beta_2 M_1) + s_4 (\bar{V}_2 \bar{M}_3 + \bar{V}_3 \bar{M}_2) + \\ \quad \left(P_1 |M_1|^2 + P_2 (|M_2|^2 + |M_3|^2) \right) M_1, \\ (\phi + \varphi) \left(\frac{\partial V_2}{\partial T_1} + \frac{\partial M_2}{\partial T_2} \right) = s_3 (\beta_1 V_2 + \beta_2 M_2) + s_4 (\bar{V}_1 \bar{M}_3 + \bar{V}_3 \bar{M}_1) + \\ \quad \left(P_1 |M_2|^2 + P_2 (|M_1|^2 + |M_3|^2) \right) M_2, \\ (\phi + \varphi) \left(\frac{\partial V_3}{\partial T_1} + \frac{\partial M_3}{\partial T_2} \right) = s_3 (\beta_1 V_3 + \beta_2 M_3) + s_4 (\bar{V}_1 \bar{M}_2 + \bar{V}_2 \bar{M}_1) + \\ \quad \left(P_1 |M_3|^2 + P_2 (|M_1|^2 + |M_2|^2) \right) M_3, \end{cases} \quad (3.19)$$

where

$$\begin{aligned} s_3 &= \phi - 2\beta_T^{(2)} - \frac{2\phi\varphi}{(\beta_T^{(2)})^2}, \\ s_4 &= 2(1, \varphi) \begin{pmatrix} s_1 \\ s_2 \end{pmatrix}, \\ P_1 &= \left(m_1 q_1 + m_2 b_1 + \frac{B_1}{2} \right) + \varphi \left(m_1 q_2 + m_2 b_2 + \frac{B_2}{2} \right), \\ P_2 &= (n_1 q_1 + n_2 b_1 + B_1) + \varphi (n_1 q_2 + n_2 b_2 + B_2), \\ m_1 &= u_0 + u_{11}, \quad m_2 = v_0 + v_{11}, \\ n_1 &= u_0 + u_{mn}, \quad n_2 = v_0 + v_{mn}, \\ q_1 &= f_{uu}\phi + \frac{1}{2}(f_{uv} + f_{vu}), \quad b_1 = f_{vv} + \frac{1}{2}(f_{uv} + f_{vu})\phi, \\ q_2 &= g_{uu}\phi + \frac{1}{2}(g_{uv} + g_{vu}), \quad b_2 = g_{vv} + \frac{1}{2}(g_{uv} + g_{vu})\phi, \end{aligned}$$

$$\begin{aligned} B_1 &= f_{uuu}\phi^3 + (f_{uuv} + f_{uvu} + f_{vuu})\phi^2 + (f_{uuv} + f_{vuv} + f_{vvu})\phi + f_{vvv}, \\ B_2 &= g_{uuu}\phi^3 + (g_{uuv} + g_{uvu} + g_{vuu})\phi^2 + (g_{uuv} + g_{vuv} + g_{vvu})\phi + g_{vvv}. \end{aligned}$$

The solution of the reaction-diffusion system (1.2) at the Turing instability critical point has the following form

$$\begin{pmatrix} u \\ v \end{pmatrix} = \begin{pmatrix} \phi \\ 1 \end{pmatrix} \left(\sum_{j=1}^3 Z_j \exp(i\mathbf{k}_j \cdot \mathbf{r}) + \sum_{j=1}^3 \bar{Z}_j \exp(-i\mathbf{k}_j \cdot \mathbf{r}) \right). \quad (3.20)$$

Combining (3.4), (3.11), (3.17) and (3.20), the amplitude Z_j can be transformed into the following form $Z_j = \varepsilon M_j + \varepsilon^2 V_j + o(\varepsilon^3)$. Determined by the expressions of Z_j and Eqs. (3.7), (3.11), (3.16) and (3.19) we can obtain the equation for the amplitude corresponding to Z_1 as follows

$$\tau_0 \frac{\partial Z_1}{\partial t} = \mu Z_1 + d \bar{Z}_2 \bar{Z}_3 - \left(w_1 |Z_1|^2 + w_2 |Z_2|^2 + |Z_3|^2 \right) Z_1, \quad (3.21)$$

where

$$\begin{aligned} \tau_0 &= \frac{\phi + \varphi}{s_3 \beta_T^{(2)}}, \quad \mu = \frac{\beta - \beta_T^{(2)}}{\beta_T^{(2)}}, \quad d = \frac{s_4}{s_3 \beta_T^{(2)}}, \\ w_1 &= -\frac{P_1}{s_3 \beta_T^{(2)}}, \quad w_2 = -\frac{P_2}{s_3 \beta_T^{(2)}}. \end{aligned}$$

Analogously, we can derive two other amplitude equations

$$\begin{cases} \tau_0 \frac{\partial Z_2}{\partial t} = \mu Z_2 + d \bar{Z}_1 \bar{Z}_3 - \left(w_1 |Z_1|^2 + w_2 (|Z_2|^2 + |Z_3|^2) \right) Z_2, \\ \tau_0 \frac{\partial Z_3}{\partial t} = \mu Z_3 + d \bar{Z}_1 \bar{Z}_2 - \left(w_1 |Z_1|^2 + w_2 (|Z_2|^2 + |Z_3|^2) \right) Z_3. \end{cases} \quad (3.22)$$

Using the polar coordinate transform

$$Z_j = \rho_j \exp(i\varphi_j) \quad (j = 1, 2, 3),$$

where $\rho = |Z_j|$, and φ_j is the polar angle. Then substituting (3.21) into (3.22), the system (3.22) becomes

$$\begin{cases} \tau_0 \frac{\partial \theta}{\partial t} = -d \frac{\rho_1^2 \rho_2^2 + \rho_1^2 \rho_3^2 + \rho_2^2 \rho_3^2}{\rho_1 \rho_2 \rho_3} \sin \theta, \\ \tau_0 \frac{\partial \rho_1}{\partial t} = \mu \rho_1 + d \rho_2 \rho_3 \cos \theta - w_1 \rho_1^3 - w_2 \left(|\rho_2|^2 + |\rho_3|^2 \right) \rho_1, \\ \tau_0 \frac{\partial \rho_2}{\partial t} = \mu \rho_2 + d \rho_1 \rho_3 \cos \theta - w_1 \rho_2^3 - w_2 \left(|\rho_1|^2 + |\rho_3|^2 \right) \rho_2, \\ \tau_0 \frac{\partial \rho_3}{\partial t} = \mu \rho_3 + d \rho_2 \rho_1 \cos \theta - w_1 \rho_3^3 - w_2 \left(|\rho_1|^2 + |\rho_2|^2 \right) \rho_3, \end{cases} \quad (3.23)$$

where

$$\theta = \theta_1 + \theta_2 + \theta_3.$$

From the first equation of the system (3.23), there are only two conditions to consider: $\theta = 0$ or π . The system (3.23) is stable for $\theta = 0$, $d > 0$ and $\theta = \pi$, $d < 0$. Hence, the system (3.23) can be reduced to the following form

$$\begin{cases} \tau_0 \frac{\partial \rho_1}{\partial t} = \mu \rho_1 + |d| \rho_2 \rho_3 - w_1 \rho_1^3 - w_2 (\rho_2^2 + \rho_3^2) \rho_1, \\ \tau_0 \frac{\partial \rho_2}{\partial t} = \mu \rho_2 + |d| \rho_1 \rho_3 - w_1 \rho_2^3 - w_2 (\rho_1^2 + \rho_3^2) \rho_2, \\ \tau_0 \frac{\partial \rho_3}{\partial t} = \mu \rho_3 + |d| \rho_1 \rho_2 - w_1 \rho_3^3 - w_2 (\rho_1^2 + \rho_2^2) \rho_3. \end{cases} \quad (3.24)$$

As the results in the [17, 22, 24], by studying the existence and stability of the equilibrium points of the amplitude system (3.24), we know that the amplitude system (3.24) has five types of steady-state solutions with the following conclusions:

- (1) The amplitude system (3.24) has an equilibrium $E_1 = (0, 0, 0)$, which is stable for $\mu < \mu_2$ and unstable for $\mu > \mu_2$;
- (2) When $\mu w_1 > 0$, the amplitude system (3.24) has an equilibrium $E_2 = \left(\sqrt{\frac{\mu}{w_1}}, 0, 0\right)$, which is stable for $\mu > \mu_3$ with $w_2 > w_1 > 0$;
- (3) When $w_1 + 2w_2 > 0$, $\mu_1 < \mu < 0$ or $w_1 + 2w_2 < 0$, $\mu < 0$, the system (3.24) has an equilibrium $E_3^{(0)} = (\rho_1^*, \rho_1^*, \rho_1^*)$ with $\rho_1^* = \frac{|d| - \sqrt{d^2 + 4\mu(w_1 + 2w_2)}}{2(w_1 + 2w_2)}$, which is always unstable;
- (4) When $w_1 + 2w_2 > 0$, $\mu_1 < \mu$, the system (3.24) has an equilibrium $E_3^{(\pi)} = (\rho_2^*, \rho_2^*, \rho_2^*)$ with $\rho_2^* = \frac{|d| + \sqrt{d^2 + 4\mu(w_1 + 2w_2)}}{2(w_1 + 2w_2)}$, which is stable for $-2w_2 < w_1 \leq p_2$, $\mu_1 < \mu < \mu_4$ or $-\frac{1}{2}w_2 < w_2 < w_1$, $\mu_1 < \mu$;
- (5) When $w_2 > w_1 > 0$, $\mu > \mu_3$ or $w_1 < w_2 < 0$, $\mu < \mu_3$, the system (3.24) has an equilibrium $E_4 = (\rho_3^*, \rho_4^*, \rho_4^*)$ with $\rho_3^* = \sqrt{\frac{|d|}{w_2 - w_1}}$ and $\rho_4^* = \sqrt{\frac{\mu - w_1 \rho_1^{*2}}{w_1 + w_2}}$, which is always unstable;

where

$$\mu_1 = \frac{-d^2}{4(w_1 + 2w_2)}, \quad \mu_2 = 0, \quad \mu_3 = \frac{d^2 w_1}{(w_2 - w_1)^2}, \quad \mu_4 = \frac{2w_1 + w_2}{(w_2 - w_1)^2} d^2.$$

By [Theorem 2.2](#), Turing instability occurs at $\beta \in (\beta_T^{(2)}, 1)$ for the system (1.2), that is $\mu = \frac{\beta - \beta_T^{(2)}}{\beta_T^{(2)}} > 0$. However, in this case, $E_3^{(0)}$ does not exist. According to the results in [17, 24], the existence and stability of the equilibria of the amplitude system (3.24) correspond to the type of spatial patterns of the original system (1.2). E_1 and $E_3^{(\pi)}$ correspond to the spot patterns, E_2 and E_4 correspond to the the stripe patterns and the mixed patterns, respectively. In addition, it is easy to know from the above discussion that $\mu_1 < \mu_2 < \mu_3 < \mu_4$. Consequently, one obtains the following results:

- (1) The system (3.24) only has a equilibrium $E_3^{(\pi)}$ for $\mu_2 < \mu < \mu_3$, which is stable, therefore, the system (1.2) only appear spot patterns;
- (2) When β crosses a critical value so that $\mu_3 < \mu < \mu_4$, the system (3.24) has two equilibria E_2 and $E_3^{(\pi)}$, correspondingly, the system (1.2) can occurs mixed patterns;
- (3) When $\mu_4 < \mu$, the system (3.24) only has a equilibrium E_2 , and then, stripe patterns will appear in the system (1.2).

Therefore, we are able to establish a connection between the initial reaction-diffusion equation and the amplitude equation presented in [Table 3.1](#). This linkage not only sheds light on the underlying mechanisms of these mathematical models, but also provides a valuable theoretical framework for further research in this field of study [17].

In this subsection, we derive the amplitude equation (3.24) of the system (1.2) using the weakly nonlinear analysis method and obtain the conditions for the appearance of different Turing patterns. In the next subsection, we will verify theoretical analysis by numerical simulation.

Amplitude system (3.24)	The original system (1.2)
E_1	Spot pattern
E_2	Stripe pattern
$E_3^{(\pi)}$	Spot pattern
E_4	Mixed pattern

Table 3.1: The correspondence between the amplitude system and the original system.

3.2 Numerical simulations of pattern formation

In this subsection, we will perform numerical simulations to verify the last part of the theoretical analysis. Taking the Parameters $\sigma_1 = 0.5$, $\sigma_2 = 3.6$, then we have

$$k_T^2 = 0.6706, \quad \beta_T^{(2)} = 0.8095.$$

According to [Theorem 2.2](#), Turing pattern will appear when $\beta \in (0.8095, 1)$. Then we choose $\beta = 0.99$, and with simple calculations, the following results can be obtained

$$d = -0.4661, \quad w_1 = 0.2653, \quad w_2 = 0.6939,$$

$$\mu_1 = -0.0329, \quad \mu_2 = 0, \quad \mu_3 = 0.3137, \quad \mu_4 = 1.4480, \quad \mu = 0.2230.$$

Hence, $\mu_2 < \mu < \mu_3$, the parameter values $\rho_2^* = 1.2414$, $-2w_2 = -1.3878 < w_1 < \rho_2$, and $E_3^{(\pi)} = (1.2414, 1.2414, 1.2414)$ represent a specific range of conditions that correspond to the fourth steady-state solution of the amplitude equation (as defined in (4)). Based on our previous analysis, the appearance of spot patterns in the reaction-diffusion system (1.2) is expected under these conditions (see [Figure 3.1](#)). Therefore, we can conclude that the formation of spot patterns in the system is likely to occur under the specified parameter values.

Next, choosing $\beta = 0.95$, we can obtain the following results

$$d = -0.4277, \quad w_1 = 1.7657, \quad w_2 = 3.2023,$$

$$\mu_1 = -0.0056, \quad \mu_2 = 0, \quad \mu_3 = 0.1565, \quad \mu_4 = 0.5968, \quad \mu = 0.1736.$$

And then get $\mu_3 < \mu < \mu_4$, $\rho_3^* = 0.5456$, $\rho_4^* = 0.0258$, $w_2 > w_1$, $\mu > \mu_3$, $E_4 = (0.5456, 0.0258, 0.0258)$, which falls within (5) of the steady-state solution of the amplitude equation. Based on the analysis in the previous section, this situation can induce the formation of the mixed patterns (the coexistence of spot patterns and stripe patterns) of the system (1.2) (see [Figure 3.2](#)).

In the following, reducing β to $\beta = 0.85$, by a series of calculations, we get

$$d = -0.0389, \quad w_1 = 1.1113, \quad w_2 = 2.4493,$$

$$\mu_1 = -0.0001, \quad \mu_2 = 0, \quad \mu_3 = 0.0009, \quad \mu_4 = 0.0039, \quad \mu = 0.0500.$$

And thus obtain $\mu > \mu_4$. The system (1.2) exhibits stripe patterns (see [Figure 3.3](#)), as predicted by previous theoretical findings, when the following conditions are met: $\rho_1 = 0.2121$, $\mu > \mu_3$, $w_2 > w_1 > 0$, $\mu w_1 = 0.0556 > 0$, and $E_2 = (0.2121, 0, 0)$. The corresponding steady-state solution of the amplitude equation is denoted as (2). From the above analysis, [Table 3.2](#) was derived.

Parameters of the Amplitude Equation									
$(\sigma_1, \sigma_2, \beta)$	d	w_1	w_2	μ_1	μ_2	μ_3	μ_4	μ	type
(0.5, 3.6, 0.99)	-0.4661	0.2653	0.6939	-0.0329	0	0.3137	1.4480	0.2230	Spot
(0.5, 3.6, 0.95)	-0.4277	1.7657	3.2023	-0.0056	0	0.1565	0.5968	0.1736	Mixed
(0.5, 3.6, 0.85)	-0.0389	1.1113	2.4493	-0.0001	0	0.0009	0.0039	0.0500	Stripe

Table 3.2: Different parameters and corresponding patterns.

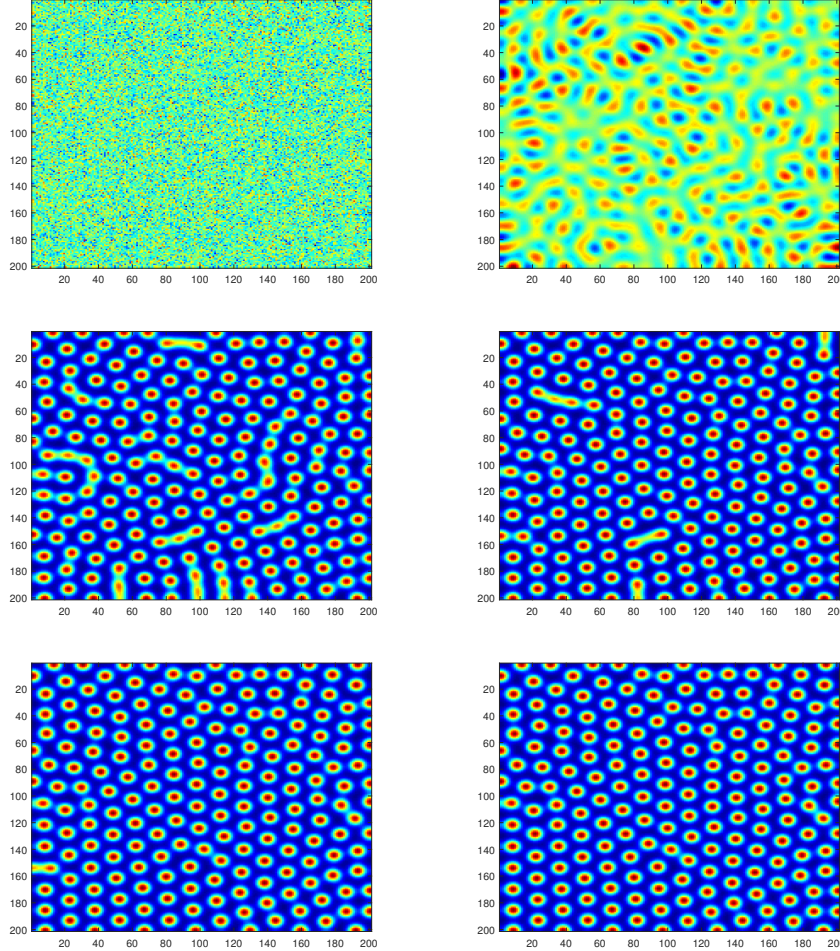


Figure 3.1: The evolutionary process of concentration of the activator u with $\sigma_1 = 0.5$, $\sigma_2 = 3.6$, $\beta = 0.99$ at $t = 0$, $t = 100,000$, $t = 750,000$, $t = 2,000,000$, $t = 2,500,000$, $t = 3,000,000$, respectively.

In order to solve the system of continuous reaction-diffusion equations (1.2) with MatLab, it is necessary to discretize the system (1.2) in space and time. Therefore, we choose $\Omega = [0, 200] \times [0, 200]$ as the discrete region, while choosing a time step $\Delta t = 0.0005$ and a space step $\Delta h = 0.5$. Since the concentration spatial pattern of the activator u is similar to the inhibitor v , we only show the concentration spatial pattern of the activator u , as shown in Figure 3.1–Figure 3.3. Next, numerical simulations are performed in the vicinity of the Turing bifurcation.

In Figure 3.1, $\beta = 0.99 \in (0.8095, 1)$ and then we have $\mu \in (\mu_2, \mu_3)$. The results show that the spot patterns and stripe patterns coexist as time t increases, but these patterns will

gradually disappear as time t changes, eventually, the spot patterns will dominate the whole region. Theoretical and numerical results are kept consistent. Here, we take $t = 0, 100,000, 750,000, 2,000,000, 2,500,000,$ and $3,000,000,$ respectively, with the following initial values

$$\begin{cases} u(x, y, 0) = u_* - 0.0002 \cdot \text{randn}(200) \\ v(x, y, 0) = u_* - 0.0002 \cdot \text{randn}(200) \end{cases} \quad (3.25)$$

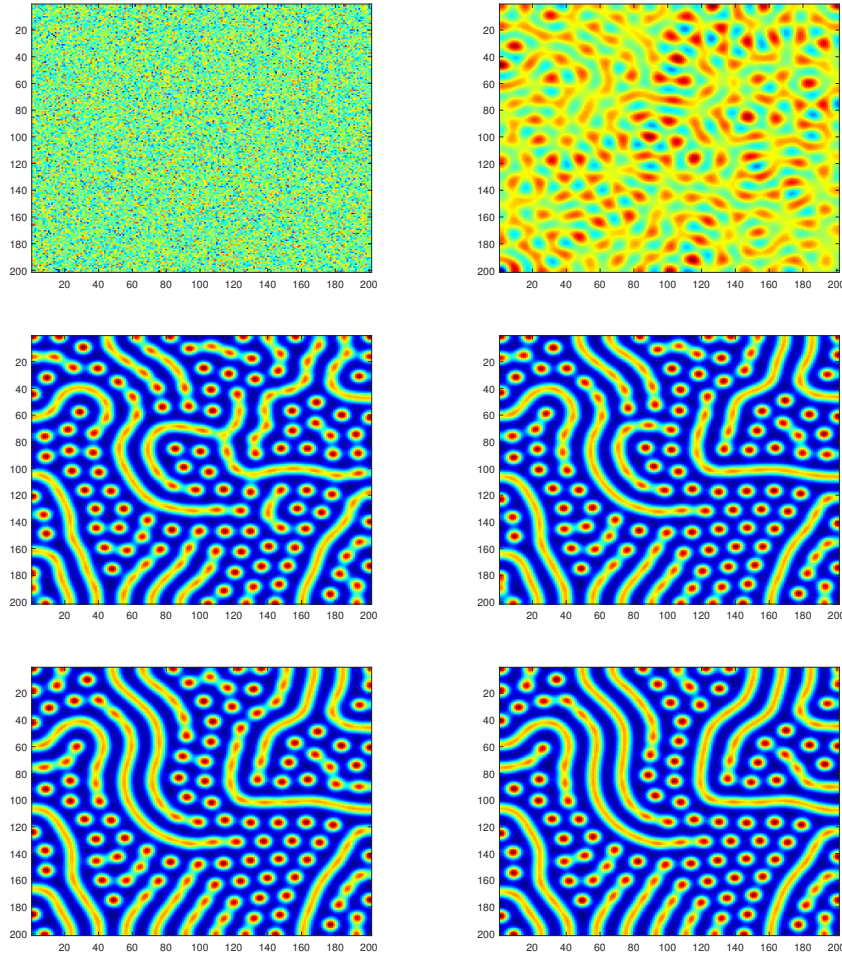


Figure 3.2: The evolutionary process of concentration of the activator u with $\sigma_1 = 0.5, \sigma_2 = 3.6, \beta = 0.95$ at $t = 0, t = 150,000, t = 750,000, t = 1,400,000, t = 2,000,000, t = 3,000,000,$ respectively.

Figure 3.2 shows the spatial pattern evolution of the activator u at $t = 0, 150,000, 750,000, 1,400,000, 2,000,000,$ and $3,000,000$ for the reaction-diffusion system (1.2) under the initial condition (3.25), and $\beta = 0.95 \in (0.8095, 1), \mu \in (\mu_3, \mu_4)$. Based on the above theoretical analysis, in this case, there is the coexistence of the spot patterns and stripe patterns. Numerically, it can be seen that this random distribution leads to the coexistence of these two patterns and this coexistence does not change further with increasing time t .

Under the same initial value conditions as above, taking $t = 0, 90,000, 1,550,000, 2,000,000, 2,800,000,$ and $3,000,000, \beta = 0.85 \in (0.8095, 1),$ then $\mu \in (\mu_4, \infty)$. With the increase of time t , the spot-stripe coexistence pattern starts to lose stability, and the stripe

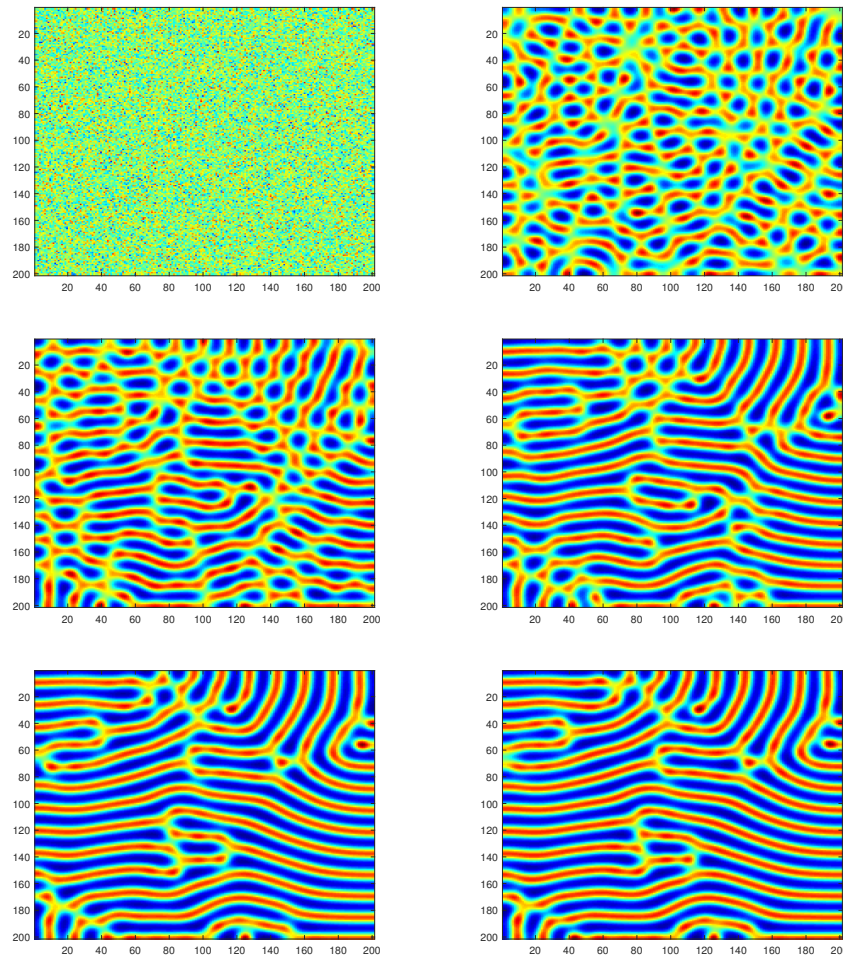


Figure 3.3: The evolutionary process of concentration of the activator u with $\sigma_1 = 0.5$, $\sigma_2 = 3.6$, $\beta = 0.85$ at $t = 0$, $t = 90,000$, $t = 1,550,000$, $t = 2,000,000$, $t = 2,800,000$, $t = 3,000,000$, respectively.

pattern appears and eventually stabilizes. The numerical simulation results (as shown in Figure 3.3) are inconsistent with the theoretical analysis.

From the results of numerical simulations, we can see that when the decay rate of the activator β decreases from 0.99, 0.95 to 0.85 in order, the type of activator concentration u pattern changes from spot patterns, spot-stripe patterns to stripe patterns in order. This indicates that the decay rate of the activator β affects the type of activator concentration u patterns. Therefore, in chemical reactions, we can adjust the decay rate of the activator β to make the concentration of the activator u tend to different patterns at dynamic equilibrium.

4 Conclusions

In this paper, the Hopf bifurcations, Turing instability, and pattern formation of Gierer–Meinhardt activator-inhibitor models with mutual resistance effects are investigated. The existence and stability of the positive equilibrium point E_* are analyzed firstly, which are influenced by the parameter β , indicating that the decay rate of the activator has an essential

effect on the system. Then the conditions for the Hopf bifurcation as well as the Turing bifurcation are established theoretically, and the effects of parameter β on the Hopf bifurcation and Turing bifurcation are discussed numerically.

It is shown that under certain conditions, a diffusion-driven Turing instability occurs at the positive equilibrium point E_* . For a fixed σ_1 , the Turing instability region in the $\beta - \sigma_2$ plane is surrounded by the Hopf bifurcation curve and the Turing bifurcation curve (see Figure 2.2). It can be concluded that there is no Turing instability for the higher decay rate of the activator.

For studying and analyzing the dynamic behavior near the Turing bifurcation, the corresponding amplitude equations are driven for the system (1.2) near the Turing bifurcation point by the weakly nonlinear analysis method, which can be used to predict the stability of the spatial pattern and its type. Based on theoretical analysis, the system will appear with spot patterns, mixed patterns, and stripe patterns, which can be verified by numerical simulations in the subsection 3.2. The results show that, with β as the adjustment parameter, the spatial patterns in the Turing instability region change from the spot patterns, and spot-stripe coexistence patterns to stripe patterns in order. These spatial patterns can not only simulate and explain the chemical oscillations between activator concentrations and inhibitor concentrations in a better way but they can also be applied to medical tests [10].

Acknowledgements

The authors would like to thank the editors and the anonymous reviewers for their valuable comments. This work is supported by the Natural Science Foundation of Tianjin City (No. 20JCQNJC00970), and the National Natural Science Foundation of China (Nos. 11701410 and 12001397).

References

- [1] S. ABDELMALEK, S. BENDOUKHA, B. REBIAI, On the stability and nonexistence of Turing patterns for the generalized Lengyel–Epstein model, *Math. Methods Appl. Sci.* **40**(2017), No. 18, 6295–6305. <https://doi.org/10.1002/mma.4457>; MR3742066; Zbl 1387.35331
- [2] R. ASHEGHI, Stability and Hopf bifurcation analysis of a reduced Gierer–Meinhardt model, *Internat. J. Bifur. Chaos Appl. Sci. Engrg.* **31**(2021), No. 10, Paper No. 2150149, 21 pp. <https://doi.org/10.1142/S0218127421501492>; MR4299204; Zbl 1473.35030
- [3] B. BOZZINI, G. GAMBINO, D. LACITIGNOLA, S. LUPO, M. SAMMARTINO, I. SGURAD, Weakly nonlinear analysis of Turing patterns in a morphochemical model for metal growth, *Comput. Math. Appl.* **70**(2015), No. 8, 1948–1969. <https://doi.org/10.1016/j.camwa.2015.08.019>; MR3400498; Zbl 1443.82017
- [4] J. CRANK, *The mathematics of diffusion*, Oxford University Press, 1979. <https://doi.org/10.1111/j.1813-6982.1940.tb02267.x>
- [5] G. GAMBINO, V. GIUNTA, M. C. LOMBARDO, G. RUBINO, Cross-diffusion effects on stationary pattern formation in the FitzHugh–Nagumo model, *Discrete Contin. Dyn. Syst. Ser. B.* **27**(2022), No. 12, 7783–7816. <https://doi.org/10.3934/dcdsb.2022063>
- [6] A. H. GIERER, H. MEINHARDT, A theory of biological pattern formation, *Kybernetik* **12**(1973), No. 1, 30–39. <https://doi.org/10.1007/bf00289234>

- [7] B. I. HENRY, S. L. WEARNE, Existence of Turing instabilities in a two-species fractional reaction-diffusion system, *SIAM J. Appl. Math.* **62**(2002), No. 3, 870–887. <https://doi.org/10.1137/S0036139900375227>; MR1897726; Zbl 1103.35047
- [8] W. JIANG, Q. AN, J. SHI, Formulation of the normal form of Turing–Hopf bifurcation in partial functional differential equations, *J. Differential Equations* **268**(2020), No. 10, 6067–6102. <https://doi.org/10.1016/j.jde.2019.11.039>; MR4069013; Zbl 1435.35043
- [9] C. A. KLAUSMEIER, Regular and irregular patterns in semiarid vegetation, *Science* **284**(1999), No. 5421, 1826–1828. <https://doi.org/10.2307/2898049>
- [10] A. J. KOCH, H. MEINHARDT, Biological pattern formation: from basic mechanisms to complex structures, *Rev. Modern Phys.* **66**(1994), No. 4, 1481. <https://doi.org/10.1103/revmodphys.66.1481>
- [11] Y. LI, J. WANG, X. HOU, Stripe and spot patterns for general Gierer–Meinhardt model with common sources, *Internat. J. Bifur. Chaos Appl. Sci. Engrg.* **27**(2017), No. 02, 1750018. <https://doi.org/10.1142/s0218127417500183>; MR3626375; Zbl 1362.35043
- [12] S. LI, J. WU, Y. DONG, Turing patterns in a reaction–diffusion model with the Degn–Harrison reaction scheme, *J. Differential Equations* **259**(2015), No. 5, 1990–2029. <https://doi.org/10.1016/j.jde.2015.03.017>; MR3349427; Zbl 1323.35087
- [13] J. LIU, F. YI, J. WEI, Multiple bifurcation analysis and spatiotemporal patterns in a 1-D Gierer–Meinhardt model of morphogenesis, *Internat. J. Bifur. Chaos Appl. Sci. Engrg.* **20**(2010), No. 04, 1007–1025. <https://doi.org/10.1142/s0218127410026289>; MR2660155; Zbl 1193.35010
- [14] Z. MEI, *Numerical bifurcation analysis for reaction-diffusion equations*, Springer Science & Business Media, Vol. 28, Springer-Verlag, Berlin, 2000. <https://doi.org/10.1007/978-3-662-04177-2>; MR1772261
- [15] Q. MENG, G. LIU, Z. JIN, Hopf bifurcation in a reaction-diffusive-advection two-species competition model with one delay, *Electron. J. Qual. Theory Differ. Equ.* **2021**, No. 72, 1–24. <https://doi.org/10.14232/ejqtde.2021.1.72>, MR4389341, Zbl 1488.34454
- [16] J. D. MURRAY, *Mathematical biology: I. An introduction*, Springer, 2002. <https://doi.org/10.1023/A:1022616217603>
- [17] O. Y. QI, *Nonlinear science and the pattern dynamics introduction*, Peking University Press, Beijing, 2010.
- [18] A. RÄTZ, M. RÖGER, Turing instabilities in a mathematical model for signaling networks, *J. Math. Biol.* **65**(2012), No. 6, 1215–1244. <https://doi.org/10.1007/s00285-011-0495-4>; MR2993944; Zbl 1252.92018
- [19] C. ROBINSON, *Dynamical systems: stability, symbolic dynamics, and chaos*, CRC press, 1998. <https://doi.org/10.1112/S0024609397343616>
- [20] S. RUAN, Diffusion-driven instability in the Gierer–Meinhardt model of morphogenesis, *Nat. Resour. Model.* **11**(1998), No. 2, 131–141. <https://doi.org/10.1111/j.1939-7445.1998.tb00304.x>; MR1634318

- [21] H. E. SCHEPERS, M. MARKUS, Two types of performance of an isotropic cellular automaton: stationary (Turing) patterns and spiral waves, *Phys. A.* **188**(1992), No. 1–3, 337–343. [https://doi.org/10.1016/0378-4371\(92\)90277-w](https://doi.org/10.1016/0378-4371(92)90277-w)
- [22] D. SONG, Y. SONG, C. LI, Stability and Turing patterns in a predator–prey model with hunting cooperation and Allee effect in prey population, *Internat. J. Bifur. Chaos Appl. Sci. Engrg.* **30**(2020), No. 09, 2050137. <https://doi.org/10.1142/S0218127420501370>; MR4132018; Zbl 1448.92249
- [23] A. M. TURING, The chemical basis of morphogenesis, *Bull. Math. Biol.* **237** (1952), No. 641, 37–72. <https://doi.org/10.1098/rstb.1952.0012>; MR3363444; Zbl 1403.92034
- [24] D. WALGRAEF, *Spatio-temporal pattern formation: with examples from physics, chemistry, and materials science*, Springer, 2012. <https://doi.org/10.1007/978-1-4612-1850-0>
- [25] R. WU, Y. ZHOU, Y. SHAO, L. CHEN, Bifurcation and Turing patterns of reaction–diffusion activator–inhibitor model, *Phys. A.* **482**(2017), 597–610. <https://doi.org/10.1016/j.physa.2017.04.053>; MR3651455; Zbl 07544836
- [26] A. YADAV, S. M. MILU, W. HORSTHEMKE, Turing instability in reaction-subdiffusion systems, *Phys. Rev. E.* **78**(2008), No. 2, 026116. <https://doi.org/10.1103/physreve.78.026116>; MR2496829; Zbl 1471.35315
- [27] L. ZHANG, F. ZHANG, S. RUAN, Linear and weakly nonlinear stability analyses of Turing patterns for diffusive predator–prey systems in freshwater marsh landscapes, *Bull. Math. Biol.* **79**(2017), No. 3, 560–593. <https://doi.org/10.1007/s11538-017-0245-x>; MR3615107; Zbl 1373.92115